MNRAS 000, 1–15 (2019) Preprint 20th November 2019 Compiled using MNRAS LaTeX style file v3.0

Galaxy Zoo Builder: Four Component Photometric decomposition of Spiral Galaxies Guided by Citizen Science

Timothy Lingard[1]⋆, Karen L. Masters[2], Coleman Krawczyk[1], Chris Lintott[3], Steven Bamford,[4], Sandor Kruk,[5], Brooke Simmons,[6], Robert Simpson,[7], Robert C. Nichol,[1]

[1] *Institute of Cosmology and Gravitation, University of Portsmouth, Dennis Sciama Building, Burnaby Road, Portsmouth, PO1 3FX, UK*
[2] *Haverford College, 370 Lancaster Ave., Haverford, PA 19041, USA*
[3] *Oxford Astrophysics, Denys Wilkinson Building, Keble Road, Oxford, OX1 3RH, UK*
[4] *Centre for Astronomy & Particle Theory, School of Physics & Astronomy, University of Nottingham, Nottingham, NG7 2RD, UK*
[5] *European Space Agency, ESTEC, Keplerlaan 1, NL-2201 AZ, Noordwijk, The Netherlands*
[6] *Physics Department, Lancaster University, Lancaster, LA1 4YB, UK*
[7] *Google UK, Six, Pancras Square, London N1C 4AG*

Accepted XXX. Received YYY; in original form ZZZ

ABSTRACT

Multi-component modelling of galaxies is a valuable tool in the quantitative understanding of galaxy evolution, however it is plagued by issues with convergence, model selection and parameter degeneracies. These issues either limit it to simple models for large samples, or complex models in very small samples (a dilemma we summarize as a choice between "quality or quantity"). This paper presents a novel framework, built inside the Zooniverse citizen science platform, which enables volunteers to help crowd-source the creation of multiple component photometric models of galaxies from FITS images. We test if this method can help solve the quandry over choosing "quality" or "quantity" for complex galaxy image modelling.

We have run the method (including a final algorithmic optimization from the best crowd-sourced solution) on a sample of 198 galaxies from the Sloan Digital Sky Survey. We examine the robustness of this new method to variation in number and population of citizen scientists, as well as compare it to automated fitting pipelines. We demonstrate that it is possible to consistently recover accurate models which show good agreement with, or improve on previous models in the literature. We demonstrate that using citizen science to make selections on number of model parameters to include and their rough optimal values is a promising technique for modeling the images of complex galaxies. We release our catalogue of models to the community.

Key words: galaxies: evolution – galaxies: spiral – galaxies: photometry

1 INTRODUCTION

Disc galaxies are complex objects, containing many different components, including a disc, disc phenomena (i.e. spiral arms, bars and rings) and central, more spheroidal structures (bulges, nuclear bulges). Decomposing disc galaxies into their component structures has become an important tool for extragalactic astronomers seeking to understand the formation and evolution of the galaxy population (e.g. Simard et al. 2002a, Simard et al. 2011, Lackner & Gunn 2012, Kruk et al. 2017, Bamford et al. 2011, Gadotti 2011, Mendez-Abreu et al. 2016, Park et al. 2007, Salo et al. 2015).

These fully quantitative methods allow researchers to obtain structural parameters of galaxy sub-components, which are useful in a variety of astrophysical and cosmological research. For example, the stellar mass found in discs and bulges places strong constraints on the galaxy merger tree from ΛCDM N-body simulations (Hopkins et al. 2010); the strength of a galaxy's classical bulge is thought to be tied to the strength of a merger event in its past (Kormendy et al. 2010); different spiral arm formation theories vary in their predictions of spiral morphology (Dobbs & Baba 2014, Pour-Imani et al. 2016, Hart et al. 2017).

⋆ E-mail: tim.lingard@port.ac.uk

The usefulness of obtaining parametric models of a galaxy has motivated the creation of many image modelling and fitting suites, including Gim2d (Simard et al. 2002b), Galfit (Peng et al. 2002), MegaMorph (Bamford et al. 2011) and Profit (Robotham et al. 2016) to name a few.

Using these tools, researchers have built large catalogues of model fits to galaxies. Perhaps most notably Simard et al. (2011) performed two-dimensional, Point-Spread-Function (PSF) convolved, two-component (bulge + disc) decomposition of 1,123,718 galaxies from the Legacy imaging of the Sloan Digital Sky Survey (hereafter SDSS) Data Release 7 (Abazajian et al. 2009). Other large catalogues of photometric fits exist: Gadotti (2011) made use of parametric multi-band light distribution modelling to model stellar bars in 300 galaxies, Mendez-Abreu et al. (2016) made use of a human-supervised approach to perform multi-component decomposition of 404 galaxies from the CALIFA survey (Sanchez et al. 2011).

However, despite the usefulness of this technique and the presence of analytic profiles and methods for modelling more complex galaxy sub-components, relatively few studies have attempted to perform large-scale (1000s of galaxies) parametric decomposition of galaxies using more complicated models than that of Simard et al. (2011). Not properly taking into account these "secondary" morphological features (such as a bar, ring and spiral arms) can impact detailed measurements of a galaxy's bulge (Gao & Ho 2017). Proper decomposition of secondary morphological features allows investigation into mechanisms behind the secular evolution of galaxies (Kruk et al. 2018, Gao et al. 2018, Head et al. 2015) and exploration of environmental effects on morphology, such as offset bars (Kruk et al. 2017).

A prominent issue when performing these detailed decompositions is the tendency for fitting functions to converge on unphysical results when not properly guided or constrained, for instance a Sérsic bulge swapping places with an exponential disc component. It is also the case that often, without near-optimal starting points, detailed model fits will fail to converge at all (Lange et al. 2016).

Another problem which needs to be addressed is whether a component should be present in the model at all. An automated fit will generally attempt to add as many components as possible to produce the closest-matching model. Many studies therefore need to select the most appropriate model by visual inspection of the resulting residuals or recovered parameters. For example, both Vika et al. (2014) and Kruk et al. (2018) inspected the resulting model and residual images for all of their parametric fits (163 and 5,282 respectively) to ensure physical results with the correct components present. The end result of most of these problems is that researchers will have to invest time to individually check many of their fits to ensure they have converged on a physical model. In the era of large sky surveys such as the SDSS (Abazajian et al. 2009), which in total imaged over 50 million galaxies, the time required to do this becomes unsustainable and introduces concerns over human error if done by only a single, or small number of individuals.

A demonstrably successful solution to the similar problem of galaxy classification in the era of large surveys, was to find a new source of person-power: Lintott et al. (2008) invited large numbers of people to classify SDSS-images of galaxies over the internet in the Galaxy Zoo project. The resulting classifications (a mean of 38 per galaxy) were then weighted and averaged to create a morphological catalogue of 893,212 galaxies. This hugely successful project, including its subsequent iterations and expansions (i.e. Willett et al. 2013, Hart et al. 2016, Willett et al. 2017, Simmons et al. 2017), has produced a large catalogue of detailed morphological classifications which are in good agreement with other studies, and have been used in a wide variety of studies of the local galaxy population (see Masters & the Galaxy Zoo Team 2019 for a recent review).

In this paper we explore an analogous solution to that Lintott et al. (2008) brought to galaxy classification for the issues faced by galaxy parametric modelling, inside the ecosystem that Galaxy Zoo set in motion (namely *The Zooniverse*[1]). We leverage citizen scientists to pick model components and perform model optimization in an online, web-browser environment[2]. We describe our method in Section 2, including details of the images and ancilliary data from SDSS as well as the strategy used to obtain scientifically useful models from volunteer classifications. We provide consistency checks within our infrastructure and to other methods in Section 3.

Where necessary, we make use of $H_0 = 70\ \mathrm{km\ s^{-1}\ Mpc^{-1}}$.

2 METHOD

2.1 The *Galaxy Builder* Zooniverse project

Galaxy Builder is a citizen-science project built on the Zooniverse web platform. It asks volunteers to perform detailed photometric modelling of spiral galaxies (potentially including bulge, disc, bar and spiral arm components). A project of this kind, allowing volunteers to interact with and model data, had never been attempted inside the current Zooniverse web platform before, so this project involved designing and implementing a model rendering[3] suite inside the existing Zooniverse front-end code-base. As with all citizen science solutions, we had to not only consider the accuracy of the resulting model, but also user experience and engagement in our design decisions.

The closest relative to this project within the Zooniverse ecosystem was the Galaxy Zoo: Mergers project (Holincheck et al. 2016). This project asked volunteers to help match the morphological properties of an image of merging galaxies to a plethora of restricted three-body simulations, in an attempt to identify the initial conditions that could result in the observed morphology. For part of the project, volunteers downloaded a Java applet, which would run restricted three-body simulations and generate output images. Volunteers could mainpulate the model parameters used in the simulation, and vote on simulations which matched a given galaxy merger image or shared important tidal features. A new batch of simulations could then be run and an optimal solution converged on.

[1] `https://www.zooniverse.org`
[2] `https://www.zooniverse.org/projects/tingard/galaxy-builder`
[3] We use the term rendering in a similar manner to that used for computer graphics: to calculate an image from a model or set of rules.

In many ways, this iterative workflow was very similar to that used in *Galaxy Builder*: volunteers were asked to manipulate the parameters of a complex astrophysical model in order to identify the most likely solution, in a problem space that traditional computational modelling struggles to solve. However, *Galaxy Builder* operates purely inside a web page and does not make use of additional citizen science projects for model selection (such as the Galaxy Zoo: Mergers' *merger wars* sub-project), instead using unsupervised clustering and computational optimization to identify final models.

2.1.1 Project Timeline and Development

The *Galaxy Builder* project was built inside the Zooniverse's (Simpson et al. 2014) Panoptes-Front-End[4] codebase, using Facebook's React.js[5] framework, as well as WebGL[6] to enable low-latency photometric galaxy model rendering. *Galaxy Builder* entered a Zooniverse beta in late November 2017 and after some user experience improvements and significant code reworking to meet internal standards, the project was launched as an official Zooniverse project on the 24th of April 2018.

A major challenge during development of the project was finding the right balance between keeping the interface and instructions simple enough for volunteers to understand intuitively, while also allowing the freedom and versatility to properly model galaxies. It was also a significant challenge to develop a compelling and simple tutorial for what is one of the most complex projects attempted on the Zooniverse platform. Feedback from expert users was essential to this process as part of the the typical beta trial process for Zooniverse projects[7].

2.1.2 The project interface

The *Galaxy Builder* project prompts volunteers to work through the step-by-step creation of a photometric model of a galaxy (described in detail in Section 2.4). The interface presents a volunteer with three views, which they can switch between at any time: a r-band cutout image of a spiral galaxy (see Section 2.2), the galaxy model they have created so far, and the residual between their model and image (shown in blue and yellow). A screenshot of the interface can be seen in Figure 1, where a residual image is shown.

The workflow is designed so that volunteers slowly subtract increasing amounts of light from the galaxy, as can be seen in Figure 2. A tutorial is available which contains a step-by-step guide to completing a classification. At each step volunteers are asked to first draw a simple isophote, and then make use of a series of sliders to adjust the parameters of the model component (see Section for more information).

Volunteers are also guided by a “score”, which is tied to the residuals and chosen to increase from zero to some arbitrary value depending on the galaxy; a less noisy and more easily modelled galaxy will have a higher maximum score. To map a residual image to a final score shown to volunteers we used

$$S = 100\exp\left(\frac{-A}{N}\sum_{i=0}^{N}\frac{\mathrm{arcsinh}^2\left(|\mathrm{y}_i - M_i|\ /\ 0.6\right)}{\mathrm{arcsinh}\,0.6}\right), \tag{1}$$

where N is the total number of pixels, y is the cutout of the galaxy, normalized to a maximum value of 1 ($y = \mathrm{cutout}/\max(\mathrm{cutout})$), M is the model calculated by volunteers and $A = 300$ is an arbitrary choice of scaling chosen based on a handful of test galaxies.

This score has the advantage of being easy (and fast) to generate from the residual image shown to voluteers (which was Arcsinh-scaled in a manner described by Lupton et al. 2004), however it is quite sensitive to small deviations of the model from the galaxy.

2.2 Sample Selection: Images and Ancillary Data

Galaxy Builder finds a niche with complex, multi-component galaxies. As such, the sample should be selected to have these features. The original sample proposed for the *Galaxy Builder* project aimed to mirror the *stellar mass-complete sample* in Hart et al. (2017). This was a sample of face-on spiral galaxies, with and without bars, complete in stellar mass.

The morphological information required to select spiral galaxies came from the public data release of Galaxy Zoo 2 (Willett et al. 2013, hereafter GZ2). Each response to a GZ2 morphology question is allocated a p value ranging from 0 to 1, where 0 indicates no volunteers responed positively to that question and 1 indicates all volunteers who classified that galaxy responded positively (i.e. $p_{\mathrm{bar}} = 0.5$ would indicate 50% of volunteers said a bar was present in a galaxy). Photometric measurements used for selection came from the NASA-Sloan Atlas (Blanton et al. 2011, hereafter NSA). The *stellar mass complete sample* is constructed using the set of criteria detailed in Table 1.

The *stellar mass-complete sample* was split into smaller sub-samples, each containing 100 galaxies. In an iterative process, each sub-sample was chosen to contain 60 of the lowest redshift galaxies and 40 random galaxies of those remaining in the sample. This was done to account for the unknown rate at which volunteers would provide classifications. In the first two sets of 100 galaxies, 1% of galaxies (i.e. 2 images) failed to run through the image preparation process, due to an error when attempting to montage multiple frames. The root cause of this error is unknown, but it leaves a sample of 198 galaxies with images that are considered in this paper.

2.2.1 Image and modelling metadata extraction

The galaxy data shown to volunteers in the *Galaxy Builder* project came in two forms: A gray-scale image cutout of the galaxy and a JSON file containing rendering information for the web-interface.

Both forms of data were obtained using a similar process:

- A montage of multiple r-band corrected frames from the

[4] `http://github.com/zooniverse/Panoptes-Front-End`
[5] `https://reactjs.org/`
[6] `https://www.khronos.org/webgl/`
[7] `https://help.zooniverse.org/best-practices/`

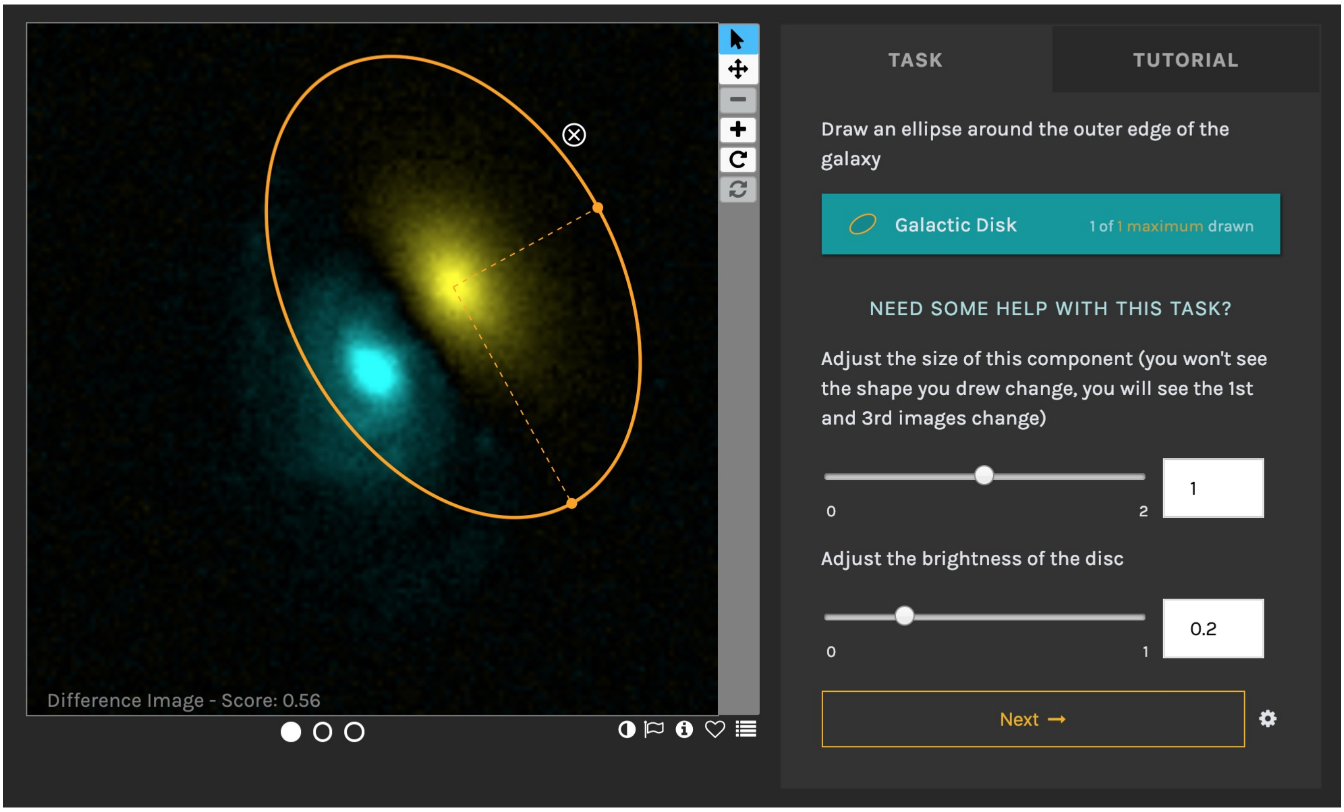

Figure 1. The *Galaxy Builder* interface. The residual image is being shown, and the volunteer is on the "Disc" task. The drawn disc component (yellow) is offset from the galaxy image (blue) to demonstrate the positive and negative residuals. Where the image equals the model the residual is black. The dots below the residual image allow the user to switch images. The icons to the right allow panning and zooming of the image (rotation was not functional for this project). The icons to the bottom right of the image allow colour inversion of the galaxy cutout, flagging of the image as inappropriate, inspection of galaxy metadata (i.e. sky position, link to SDSS SkyServer), ability to save the image as a favourite and to add to a Zooniverse "collection". The Score shown in the bottom left of the image is calculated using Equation 1 and is a rough goodness-of-fit measure.

Table 1. The selection criteria used in Hart et al. (2017) to create the *stellar mass-complete sample* of 6222 spiral galaxies.

Description	Value
Face-on spiral morphological selection.	GZ2 $p_{\text{features}} \cdot p_{\text{not edge on}} \cdot p_{\text{spiral}} \geq 0.5$
Redshift limits.	$0.02 < z < 0.055$
Face-on galaxy selection using g-band axial ratio.	$(b/a)_g > 0.4$
Volume correction.	$9.45 < \log(M_*/M_\odot) \leq 11.05$
Computation of stellar mass completeness limits using the method of Pozzetti et al. (2009) and limits calculated by Hart et al. (2017).	$2.07\log(z) + 12.64 < \log(M_*/M_\odot) < 2.45\log(z) + 14.05$

SDSS DR13 (Albareti et al. 2017) data release was created. To combine multiple FITS images, we made use of Astropy (The Astropy Collaboration et al. 2018), and the MONTAGE (Jacob et al. 2010) software package.

- This montage was cropped to four times the Petrosian radius of the galaxy.
- The SEXTRACTOR software (Bertin & Arnouts 1996) was used to identify regions containing secondary sources (foreground stats, other galaxies) and generate a mask.
- A PSF was obtained from the relevant Sloan r-band `psField` file, extracted at the central position of the galaxy (Stoughton et al. 2002).
- The JSON file was written containing the cut-out data and the 2D boolean mask obtained from the source extraction process. This file also contained other metadata needed for the rendering process (PSF, the size of the PSF array, and the width and height of the image).
- Another JSON file containing simply the information used to render the volunteer's model (image size and PSF) was created.
- An arcsinh-stretch was applied to the masked cutout (as described by Lupton et al. 2004). It was then saved as a grey-scale image.

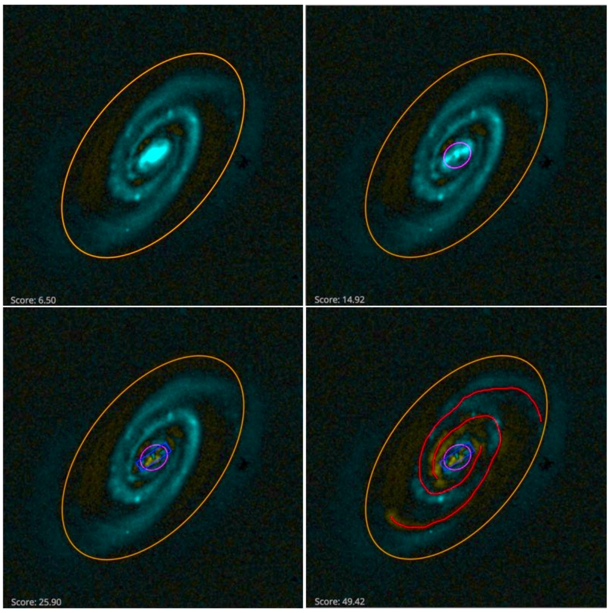

Figure 2. Figure demonstrating the desired result of each step of the modelling process, as seen from the residual image provided to volunteers. The top left panel shows the galaxy after only a disc component has been added: the top right contains a disc and a bulge; the bottom left has a disc, bulge and bar; the bottom right is the finished model with a disc, bulge, bar and spiral arms. The images shown is SDSS J104238.12+235706.8. This brightness and contrast of this image have been edited to improve visibility in print.

The decision to use r-band images in our subject set was due to its higher signal-to-noise than other bands.

Once a sub-sample had been created, the Zooniverse's PANOPTES-PYTHON-CLIENT[8] was used to upload them as a subject-set to the Zooniverse.

A separate stacked image and sigma image was calculated for the r-band corrected frames present in the montage, as described in Appendix B. These were not caluclated using MONTAGE as its reprojection step does not conserve errors. These images were not shown to volunteers but were used for model tuning and comparison.

2.3 Choice of Retirement limit

Initially, 10 classifications were collected per galaxy, however preliminary analysis indicated this number of independent answers was insufficient to create reliable and reproducable aggregate classifications. For this reason, a hand-picked sample of 56 galaxies was then re-activated with a retirement limit of 30 classifications per galaxy. This sample was chosen by eye to be a relatively diverse set of galaxies, most with prominent spiral features including grand-design and flocculent arms. Its purpose was to allow the development of the aggregation methodology.

Once this hand-picked sample was completed, and it had been determined that 30 classifications per galaxy was sufficient, the remaining galaxies from the initial two sub-samples were re-activated, as well as a repeat of the first sub-sample (hereafter the *validation subset*) to measure volunteer consistency. This paper focuses on these 198 galaxies (presented in *Galaxy Builder* as 296 separate images) in order to explain the method used, and test the reliability of the models obtained. The *Galaxy Builder* project is still active on the Zooniverse website as of the time of writing and continues to collect classifications for further samples of galaxies.

[8] `https://github.com/zooniverse/panoptes-python-client`

2.4 The Galaxy Model

The model chosen was largely based on the components and methodology described in Peng et al. (2002). The model components consisted of:

(i) An exponential, elliptical disc.
(ii) An elliptical Sérsic bulge, with n chosen by volunteers and allowed to vary from 0.5 to 5.
(iii) A Sérsic bar with a "boxiness" modifier (as described in Peng et al. 2002).
(iv) Any number of freehand poly-line spiral arms.

Each spiral arm is modelled using a poly-line drawn by the volunteer. The brightness of a spiral arm at any point is given by the value of a Gaussian centred at the nearest point on any drawn poly-line, with volunteers able to choose the Gaussian width and peak brightness using sliders. Radial falloff was added by multiplying by the value of the previously added exponential disc, though volunteers could change the half-light radius of this falloff disc.

The modelling code ignores masked regions identified as secondary sources by SEXTRACTOR. It over-samples the bulge, disc and bar components by a factor of five and performs PSF convolution using a PSF obtained from the relevant Sloan r-band `psField` file, extracted at the central position of the galaxy (Stoughton et al. 2002).

2.5 Reprojection of Classifications into original SDSS Frame Coordinates

In order to properly account for errors and as part of the data reduction process, we transform all classifications recieved for a galaxy from the coordinate space of the MONTAGE-created cutouts back into the WCS of the original frames. This was motivated by the need for accurate sigma images, which it is not possible to create for the cutout created using MONTAGE due to the reprojection having a smoothing effect on the background noise, despite being flux-conserving overall.

2.6 Classification Aggregation Methodology

In this Section, we will use the galaxy UGC 4721, a two-armed barred spiral galaxy at $z = 0.02086$ classified by de Vaucouleurs et al. (1991) as SBcd, to illustrate the data reduction and aggregation methodology. For UGC 4721 we received 32 classifications, containing 28 discs, 24 bulges, 17 bars and 47 drawn spiral arm poly-lines. These annotations can be seen in Figure 3, overlaid on the greyscale r-band image of the galaxy.

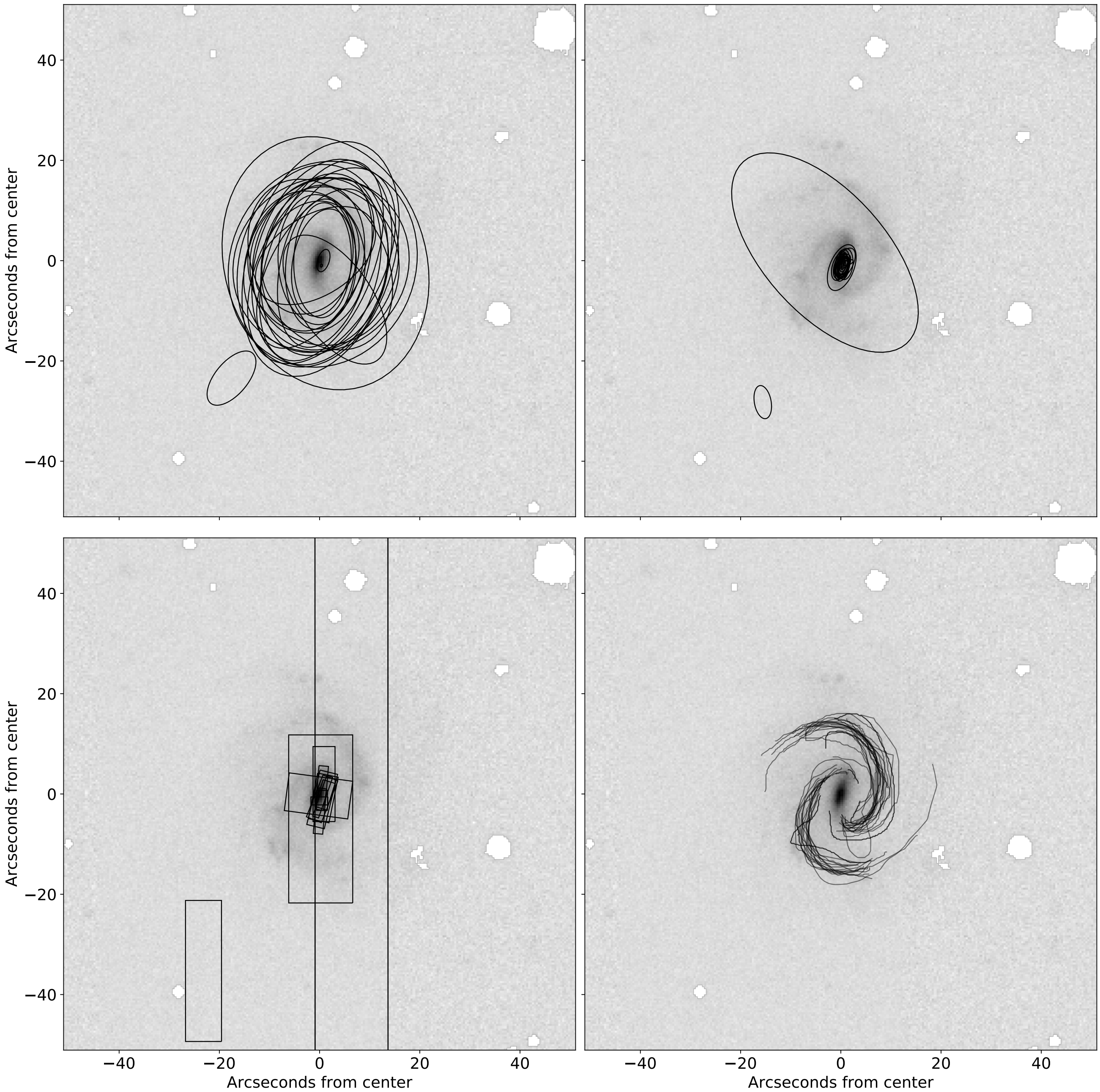

Figure 3. Components drawn by volunteers for UGC 4721. The top left panel shows drawn discs, top right shows drawn bulges, bottom left shows drawn bars and bottom right shows drawn spiral arms.

2.6.1 Best Individual Classification

As *Galaxy Builder* is primarily asking volunteers to solve a complicated regression problem, it is possible to identify the classification provided for each galaxy with the best residual, and assume that this classification has roughly found the globally optimal model. We make use of the model's χ^2_ν (Equation 2, as used by GALFIT) in units of nanomaggies, to score the volunteer models[9].

[9] Note that this is not the score shown to volunteers, Equation 1.

$$\chi^2_\nu = \frac{1}{N_{\rm dof}} \sum_{x=1}^{nx} \sum_{y=1}^{ny} \frac{(f_{\rm data}(x,y) - f_{\rm model}(x,y))^2}{\sigma(x,y)^2} \tag{2}$$

We note that it is impossible to calculate the degrees of freedom of a nonlinear model such as a Sérsic profile, and as such χ^2_ν is not an appropriate measure for model comparison (Andrae et al. 2010). We aproximate $N_{\rm dof} \sim nx \times ny$ as the number of pixels present in an image, as the number of model paramters is insignificant in comparison. Values of σ were taken from the sigma image for the galaxy.

Table 2. The clustering parameters used for the disc, bulge and bar components present in *Galaxy Builder*

component	`eps`	`min_points`
Disc	0.3	5
Bulge	0.3	3
Bar	0.385	3

2.6.2 Aggregation of Volunteer Models

As we have multiple independent answers for each parameter and component, we can also combine these to find an aggregated answer. Aggregate model calculation was done on a component-by-component basis, rather than per classification, i.e. clustering of discs was performed independently to that of bulges, bars and spirals. Clustering was performed using the Jaccard distance measure (also known as the intersect-over-union distance, or IOU distance), which is a simple metric determining the relative shared area of two shapes:

$$d_J(A, B) = 1 - \frac{|A \cap B|}{|A \cup B|}. \tag{3}$$

The algorithm chosen to perform clustering was the density-based spatial clustering of applications with noise (DBSCAN, Boonchoo et al. 2018) algorithm, due to its robustness and speed. We made use of Scikit-learn (Pedregosa et al. 2011) to implement the algorithm. In DBSCAN the core of a cluster is defined as a group of at least `min_points` that are all within a distance `eps` of each other. Additionally, any points within a distance `eps` of a cluster's core are also associated with the cluster. The values of `eps` and `min_points` for the disk and bulge were chosen by visually inspecting the resulting clustering results. The value of `eps` used to cluster bars was tuned such that the aggregate model best agreed with GZ2 $p_{\rm bar}$ ($p_{\rm bar} < 0.2$ implying no bar and $p_{\rm bar} > 0.5$ implying a definite bar). The values used can be seen in Table 2. Bar with axis ratios greater than 0.6 were removed from the pool as this was deemed unphysical.

For shapes clustered in this way, we define the aggregate component to be the shape which minimises the sum of Jaccard distances to each of the shapes in the cluster. For our example galaxy, UGC 4721, clustered and aggregate components can be seen in Figure 4.

To cluster drawn spiral arms, we define a custom separation measure to represent how far away one poly-line is from another. This measure was chosen to be the mean of the squared distances from each vertex in a poly-line to the nearest point (vertex or edge) of another poly-line, added to the mean of the squared distances from the second polyline to the first. A mathematical description of this measure can be found in Appendix A. We make use of this separation measure inside the DBSCAN algorithm to cluster these drawn lines, after removing any self-intersecting drawn arms (as this was deemed an easy method to filter out "bad" classifications).

Once spiral classifications on a galaxy have been clustered into the physical arms they represent, the points are deprojected using the axial ratio from a 2D, single-component Sérsic fit in r-band, provided in the NSA catalogue (Blanton et al. 2011). The deprojection method assumes a thin disc and stretches the elliptical minor axis to match the major axis.

Deprojected points within each drawn poly-line are converted to polar coordinates and unwound using `numpy.unwrap` to allow model fitting. These unwound points are then cleaned using the Local-outlier-factor algorithm (LOF, Breunig et al. 2000). For each arm in the cluster, the LOF algorithm was trained on all points not in that arm, and then used to predict whether each point in the arm should be considered an outlier. In this way we clean our data while respecting its grouped nature. The points removed as outliers for the example galaxy are shown in Figure. 5.

For each arm cluster in each galaxy, a logarithmic spiral model was fitted using Bayesian Ridge Regression, performed using the Scikit-learn python package. Hyperpriors on the noise parameter were chosen by fitting a truncated gamma distribution (Zaninetti 2014) to the spiral width slider values returned by volunteers (ignoring sliders left at the default or moved to the extremes of allowed values). To obtain a single value for the pitch angle of a galaxy, we take the length-weighted average pitch angle of all arms detected in the galaxy (as used by Davis & Hayes 2014).

The final galaxy model for UGC 4721 obtained through aggregation can be seen in Figure 6.

2.7 Model Tuning

As mentioned above, the need for a numerical fit to fine-tune parameters of *Galaxy Builder* models was anticipated. This tuning was performed using the L_BFGS-b algorithm (Byrd et al. 1995), implemented in SCIPY (Jones et al. 2001), to minimize the model's χ^2_ν (Equation 2). Parameter bounds were chosen to be as uninformative as possible, while preventing catastrophic fitting failure where possible. All parameter bounds can be found in Table C1. Tuning was performed on both the best individual models and the aggregate models, and the resulting χ^2_ν values were almost identical, suggesting convergence to the same minima. After tuning, some models display the problematic behaviour noted in Kruk et al. (2018), including bar ellipticity increasing beyond 0.5 and bulge and bar effective radius increasing to be larger than the disk. We note one case where the best individual model contains a bar being used to mask a point source that was not identified in the masking process.

The tuning process sucessfully lowered model χ^2_ν values to between 1 and 5 for both best individual and aggregate models. Models and residuals for the tuned best individual and aggregate models for our example galaxy are shown in Figure 7. We still see spiral structure present in the residuals, as the spiral arms were not positioned perfectly (especially the spiral start and end points). We reccommend that future methods attempt to optimize these values.

2.8 Error Estimation

The uncertainties reported by many software fitting packages (GALFIT and MEGAMORPH from the above list) are lower estimates on the real uncertainty, due to secondary sources not being modelled, flat-fielding errors and incorrect models (Peng et al. 2010). Other packages such as GIM2D

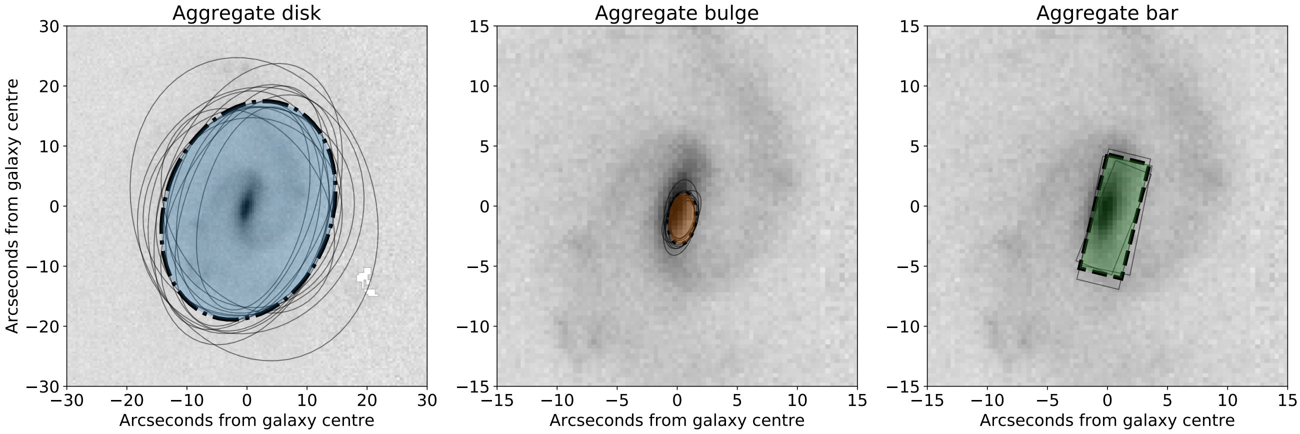

Figure 4. Calculated aggregate components for UGC 4721. The aggregate disc is shown using a dot-dashed line and blue fill in the first panel, the aggregate bulge with a dotted line and orange fill in the second panel and the aggregate bar using a dashed line and green fill in the third panel.

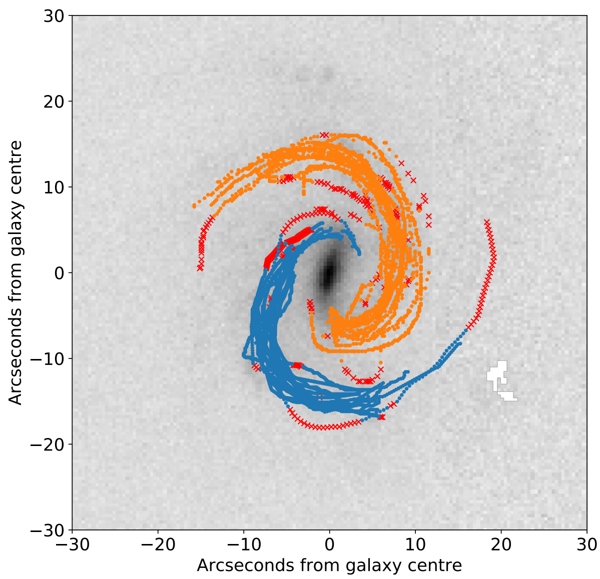

Figure 5. Point cleaning for the spiral arm clusters for UGC 4721. Points identified as outliers are displayed as red crosses, points used to fit log spirals are orange and blue dots.

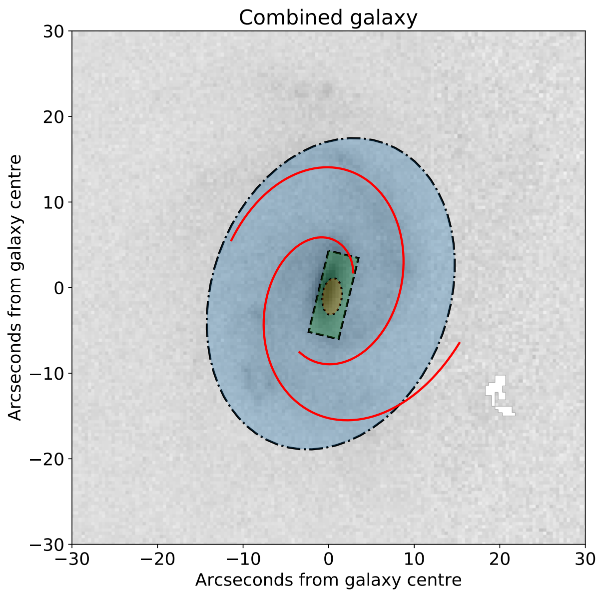

Figure 6. Resulting aggregate bulge + disc + bar + spiral arms components for UGC 4721. The disc is shown in blue with a dashed outline, the bulge in orange with a dash-dot outline, the bar in green with a dotted outline, and the spiral arms in red.

and PROFIT attempt to fully model posterior distributions and so produce more representative uncertainties, however this comes with a larger computational cost and configuration complexity.

As all shapes in a cluster can be viewed as volunteers' attempts at modelling the underlying component, the sample variance of the parameters of these shapes can be used as a good approximation of the underlying variance of the component. Figure 4 illustrates the variance in clustered shapes for our example galaxy (UCG 4721). Effective radii generally had relative errors of around 10% and axis ratios show an absoulute error of around 0.10. Parameters dictated by sliders show much larger and less consistent errors, potentially due to their impact being conceptually harder for volunteers. It is therefore possible that slider errors should be treated as a measure of volunteer confidence rather than a measure of the posterior. A table detailing all errors on parameters is provided in the appendix (Table C2).

3 RESULTS

In this Section we explore the consistency with which volunteers modelled galaxies, the variance of the aggregate model recovered and compare our recovered models to other results in the literature.

3.1 Examination of Volunteer consistency

We aggregate two independent models for a set of 98 galaxies based on "original" or repeat ("validation") classifications,

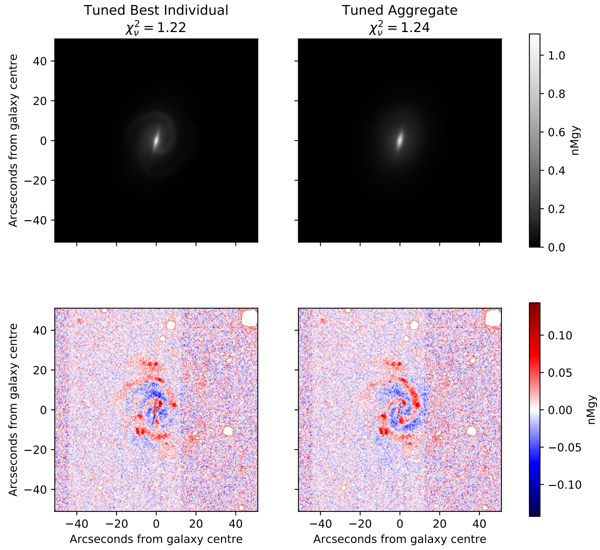

Figure 7. Tuned best individual and aggregate models, and their residuals for UGC 4721. The top two panels show the models, with the tuned best individual model on the left and the tuned aggregate model on the right. Bottom panels show the corresponding residuals, where red indicates oversubtraction of the galaxy and blue indicates undersubtraction.

obtained with the same retirement limit (see Section 2.3 for more on this selection).

One of the simplest choices the volunteers have is whether to include a model component or not. Figure 8 illustrates the consistency with which volunteers made use of a component in their model for a galaxy. We see that volunteer classification is very consistent (scatter in fraction of 0.1), with volunteers almost always using a disc and bulge, and consistent proportions agreeing on the presence of a bar and the number of spiral arms.

After selecting a component, the volunteer sets its shape and size. We see generally good consistency in isophotal shape and size, with the least consistent component is the bar, which may be caused by the lower proportion of volunteers incorporating one into their model. Visual inspection suggests that many volunteers used a very elliptical bulge and drawn spirals to capture the light from the bar. Fewer bars having been drawn by volunteers also has the effect of making clustering more difficult and more uncertain, even for a strongly barred galaxy we effectively go from receiving 30 classifications to around 12 for the bar. The variation in axial ratios and effective radii for the aggregate discs, bulges and bars are shown in Figure 9: the sample error in disc size is 3.8 arcseconds, bulge size is 1.6 arcseconds and bar size is 1.5 arcseconds. There is very little consistency in axial ratio for the bulge and bar, however the disc axial ratio shows good consistency, with a sample error of 0.064.

3.2 Best Individual vs Aggregate Model

For each galaxy in the sample we compare the tuned aggregate model to the tuned best individual model, and find that both models appear to converge on similar values of χ^2_ν. It is notable how close many volunteers' models came to the optimial solution without any tuning, however the best individual models come from a wide variety of users, not a small number of super-users. Our recommendation is to make use of the tuned aggregate model for scientific analysis. As users may wish to instead make use of a number of volunteer models as starting points for their own numerical fits we also make these available.

3.3 Comparison to results in the literature

After having obtained aggregated models for our galaxies, we examine how our models compare to other results in the literature. There exists no published comparison sample with four-component fits, instead we make comparisons for individual or subsets of model components.

3.3.1 Comparison to Galaxy Zoo morpohology

When comparing the probability of a volunteer's classification containing a bar component against a galaxy being classed as strongly-barred or as having no bar (as defined in Masters et al. 2010), we see a significant difference: classifications of strongly-barred galaxies ($p_{\rm bar} > 0.5$) had a 0.47 ± 0.14 chance of containing a bar, vs 0.30 ± 0.11 for galaxies classed as having no bar ($p_{\rm bar} < 0.2$). The Spearman correlation between GZ2's $p_{\rm bar}$ and the bar likelihood in *Galaxy Builder* is 0.56, implying a significant correlation.

3.3.2 Comparison to One-component fit - axis ratio

We compare the axis ratios of the discs of *Galaxy Builder* aggregate models (without tuning) to the axis ratio of a 2D Sérsic fit to the r-band SDSS image of each galaxy (as provided in the NSA catalog, Blanton et al. 2011).

We see excellent agreement for all types of *Galaxy Builder* models (Figure 10). For the untuned models there is an error of ~ 0.1, consistent with our expected errors (derived in Section 2.8). For the aggregate model, 23% measurements with axis ratio less than 0.6 are outside 2σ, significantly higher than the expected 5%. This is opposed to 5.0% of measurements with axis ratio greater than 0.6. There is a clustering of outlying values at $b/a = 0.5$ which is almost certainly due to the drawing tool ellipse having a default axis ratio of 0.5. Where this default is a "good enough" fit we hypothesise that volunteers are less likely to modify it, while if it needs to move a long way they find a more refined value. We see similar behaviour in the cluster of values at $b/a = 1$ representing volunteers hitting the maximum value and not refining further.

Volunteers not adjusting components from their default values was a consistent issue with untuned models (36% of all disc components drawn by volunteers were left at the default axis ratio, and over half of all bars were left with their default rotation, 12% of the best individual galaxies had disc axis ratios left at the default values). Future projects should carefully consider their interface design to minimize this bias. Tuning models successfully removes this bias, and reduces the error between *Galaxy Builder* disk axis ratios and that of the NSA Sérsic fit to 0.07 for the tuned aggregate models and 0.08 for the tuned best individual.

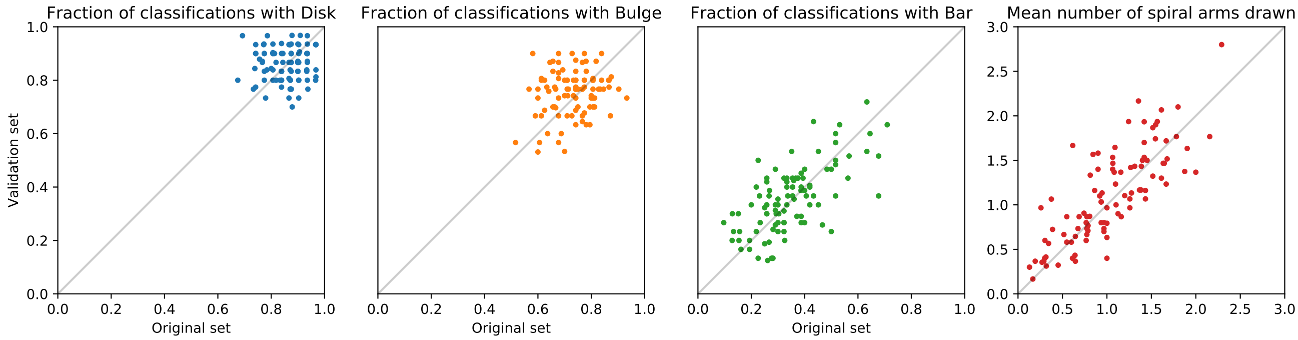

Figure 8. Comparison of frequency of use of component in volunteer models between the original and validation sets of classifications.

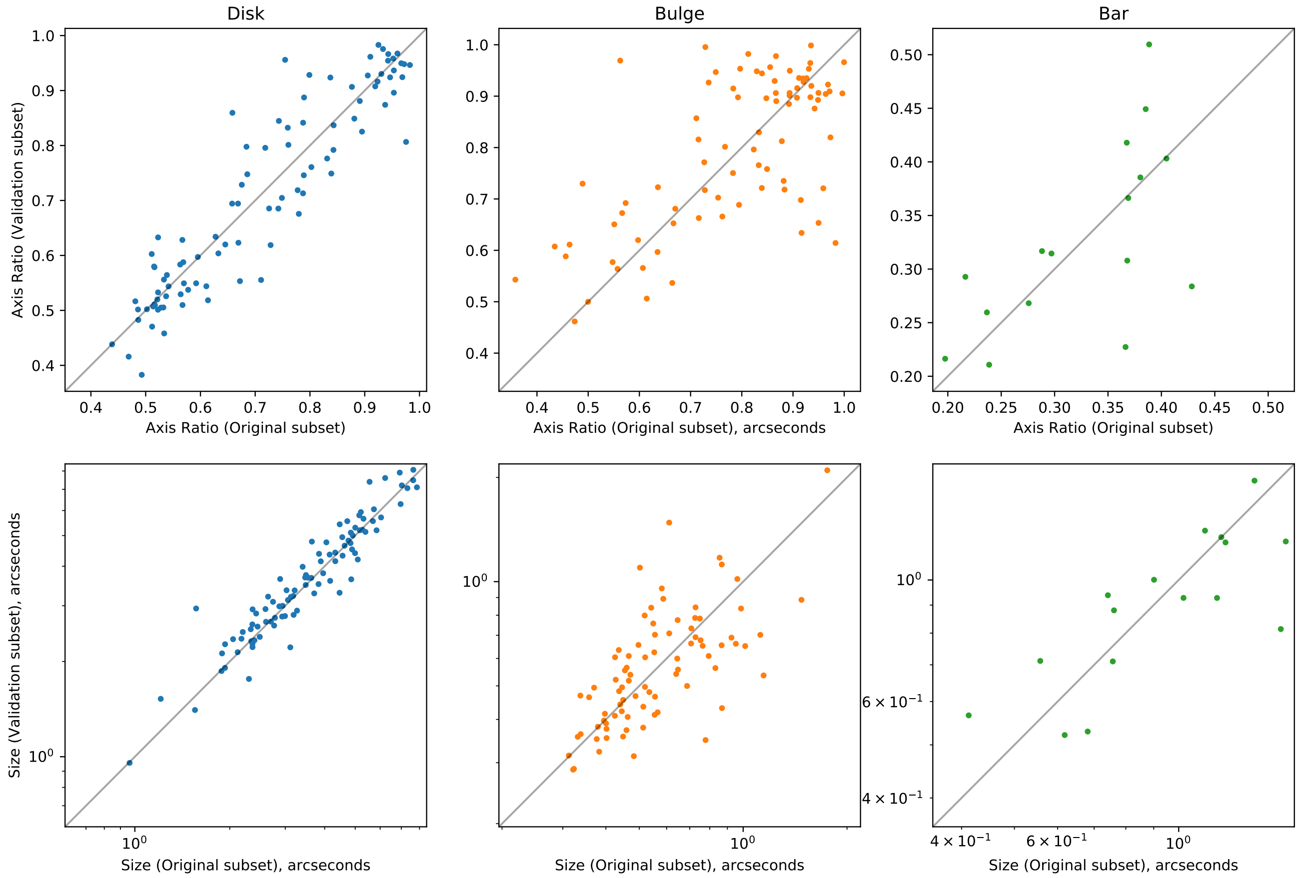

Figure 9. Comparison of component shape in aggregate models between the original and validation sets.

3.3.3 *Comparison to Disc-Bulge models*

One of the largest catalogs of 2D multi-component fits is Simard et al. (2011), which performed simultaneous, two-bandpass decompositions of 1,123,718 galaxies in the Legacy area of the SDSS DR7 using GIM2D. Three variations of models were fitted: a pure Sérsic model, an exponential disc and de-Vaucouleurs bulge model, and an exponential disc and a Sérsic bulge model. Lackner & Gunn (2012) similarly fitted two models to SDSS main-sample galaxies: an exponential disc and exponential bulge (exp+exp), and an exponential disc and de Vaucouleurs bulge (exp+dV). They used a Levenberg-Marquadt gradient descent algorithm, with initial parameters taken from previous SDSS analysis.

Comparing between these catalogues and to *Galaxy Builder* models, we see that our models show good agreement with others, when the models which are fit are comparable. Comparing bulge to total fraction, we see closest agreement to the exp+exp model, where bulge Sérsic index is similar to that most often chosen by *Galaxy Builder* volunteers, who consistently preferred to fit bulges with low Sérsic indices. Bulge measurements are very sensitive to central sub-structure and model choice (Gao & Ho 2017), so comparing B/T between models with very different bulge profiles

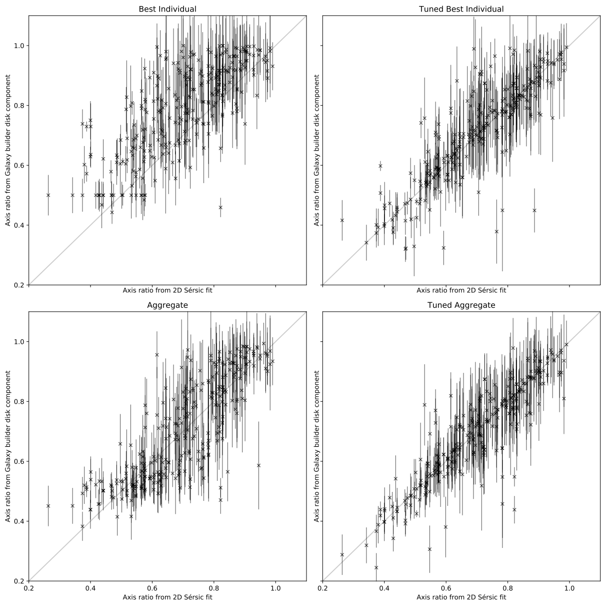

Figure 10. Difference between the axis ratios of the disc components of various *Galaxy Builder* models to the results of an r-band Sérsic profile fit.

would be expected to show a lot of scatter. The Kendall rank correlation coefficients between our measurments and all the different fits of Simard et al. (2011) and Lackner & Gunn (2012) (as well as those compared with each other) can be seen in Figure 11. The low correlation coefficients in general, even when comparing the results of fitting identical models (the two exp+dV models), illustrate the difficulty of calculating reliable bulge to total ratios for galaxies. We conclude that *Galaxy Builder* models are able to agree with simpler, more conventional photometrically fit models as well as those models agree with each other, and provide a physically motivated B/T ratio.

3.3.4 Comparison to Disc-Bulge-Bar models

Kruk et al. (2018) performed multi-component, multi-band decompositions of a selection of SDSS galaxies, 12 of which were also classified in *Galaxy Builder*. Figure 12 compares the axis ratios and effective radii of bulges, discs and bars in Kruk et al. (2018) to those present in the tuned aggregate models. We see strong agreement in disk effective radius and axis ratio, with significantly more scatter in the sizes and shapes of the central components. We hypothesize that this is caused by difficult parameter degeneracies and issues with tuning, as the aggregate model without tuning shows closer agreeement (with systematic errors in size due to the nature of the clustering).

3.3.5 Comparison to Disc-Bulge-Bar-Spiral models

To the best of our knowledge, no photometic models exist for the Galaxy Builder sample which contain spiral arm structure. The closest comparable result is that produced by Gao & Ho (2017), however the galaxies they used are not in the Sloan footprint.

In order to provide a comparison for our novel method of spiral parameter (pitch angle and amplitude) extraction, we compare the result of our logarithmic spiral fit to the relationship obtained by Hart et al. (2016) between GZ2 classification and galaxy pitch angle (Figure 13). Their fit was obtained by using the Zooniverse to filter good vs bad spiral arm segments identified using a leading automated spiral arm detection and fitting tool, SpArcFiRe (Davis & Hayes 2014), whereas *Galaxy Builder* asks volunteers to provide their own opinion on spiral arm number, location and tightness. *Galaxy Builder* pitch angles are within the uncertainties on the Hart et al. (2016) fit, even when not accounting for error on our measurements.

Many researches (Davis & Hayes 2014, Díaz-García et al. 2019 to name a few) have noted that many galaxies show large inter-arm variations in pitch angle, suggesting that obtaining a single value of a galaxy's pitch angle is highly dependent on which arms have been identified. We plan to further explore this issue in a future work.

4 SUMMARY AND CONCLUSIONS

In this paper we present a novel method for modelling of galaxy images, *Galaxy Builder*, which was conceived with the goal of solving the "quality of quantity" dilema facing galaxy image modelling, which, despite advances in computation, still typically requires significant human interaction to achieve quality fits.

Galaxy Builder leverages the power of crowd sourcing for the hardest to automate parts of image fitting, namely determining the appropriate number of model components to include, and finding regions of parameter space close to the global optima.

We have demonstrated that we are able to obtain models with comparable reduced chi-squared values (between 1 and 5) to results in the literature, using either the best individual classification provided by volunteers or an aggregate model from clustering. We obtain errors on parameters through the sample standard deviation of component clusters, which respects the complex curvature of the likelihood space better than simple jacobian approximations.

We compare these new models to existing results in the literature where available. We find good agreement where the models or parameters are comparable, and comment on instances where *Galaxy Builder* should provide superior models.

We were able to obtain models for 296 images with a rate of one galaxy per day. We note that user experience and task simplification will need to be considered if significantly larger numbers of these models are to be obtained. We note that, at the time of writing and to the best of our knowledge, the number of photometric models obtained here is significantly larger than the largest sample obtained through purely computational photometric fitting of disc, bulge, bar and spiral arms in galaxies (10 galaxies, Gao & Ho 2017, who also included rings, disc-breaks and further components).

We are optimistic about the potential of projects like *Galaxy Builder* to dramatically increase the ability of researchers to perform complex, labour-intensive modelling of galaxy photometry, leveraging the power of the crowd to

Figure 11. Correlation matrix showing Kendall rank correlation coefficient between measures of Bulge to Total fraction from *Galaxy Builder* results and other models fitted in Simard et al. (2011) and Lackner & Gunn (2012). Colours and box size indicate the strength of the correlation.

perform the complex tasks best suited to humans, and computer algorithms for the final optimization.

We release our catalogue of models to the community, and in future work we use this sample to investigate spiral arm formation mechanisms (T. Lingard et al. in prep.).

5 ACKNOWLEDGEMENTS

This publication made use of SDSS-I/II data. Funding for the SDSS and SDSS-II was provided by the Alfred P. Sloan Foundation, the Participating Institutions, the National Science Foundation, the U.S. Department of Energy, the National Aeronautics and Space Administration, the Japanese Monbukagakusho, the Max Planck Society, and the Higher Education Funding Council for England. The SDSS Web Site is `http://www.sdss.org/`.

Montage is funded by the National Science Foundation under Grant Number ACI-1440620, and was previously funded by the National Aeronautics and Space Administration's Earth Science Technology Office, Computation Technologies Project, under Cooperative Agreement Number NCC5-626 between NASA and the California Institute of Technology.

This project was partially funded by a Google Faculty Research Award to Karen Masters (`https://ai.google/research/outreach/faculty-research-awards/`), and Timothy Lingard acknowledges studentship fund-

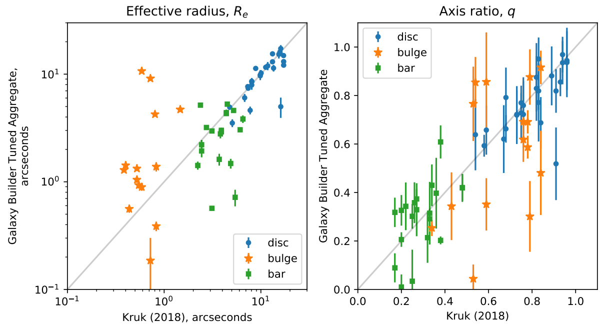

Figure 12. Comparison between *Galaxy Builder* tuned aggregate models and the result of 3-component, multiwavelength fits performed by Kruk et al. (2018). Discs, Bulges and Bars are shown as blue circles, orange stars and green squares respectively. The left panel compares component effective radius, the right panel compares the component axis ratio.

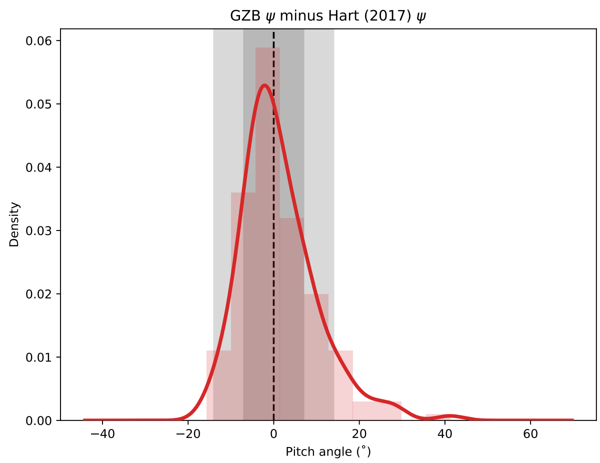

Figure 13. A comparison of Pitch angle obtained by Hart et al. (2016) with measured pitch angles for the aggregated model results in galaxies in the Galaxy Zoo Builder sample. The grey regions show 1- and 2σ errors from Hart et al. (2016). Errors on *Galaxy Builder*-measured pitch angles are not accounted for.

ing from the Science and Technology Facilities Council (ST/N504245/1).

References

Abazajian K. N., et al., 2009, ApJS, 182, 543
Albareti F. D., et al., 2017, ApJS, 233, 25
Andrae R., Schulze-Hartung T., Melchior P., 2010, arXiv e-prints, p. arXiv:1012.3754
Bamford S. P., Häußler B., Rojas A., Borch A., 2011, in Evans I. N., Accomazzi A., Mink D. J., Rots A. H., eds, Astronomical Society of the Pacific Conference Series Vol. 442, Astronomical Data Analysis Software and Systems XX. p. 479
Bertin E., Arnouts S., 1996, A&AS, 117, 393
Blanton M. R., Kazin E., Muna D., Weaver B. A., Price-Whelan A., 2011, AJ, 142, 31
Boonchoo T., Ao X., He Q., 2018, CoRR, abs/1801.06965
Breunig M. M., Kriegel H.-P., Ng R. T., Sander J., 2000, in Proceedings of the 2000 ACM SIGMOD International Conference on Management of Data. SIGMOD '00. ACM, New York, NY, USA, pp 93–104, doi:10.1145/342009.335388, `http://doi.acm.org/10.1145/342009.335388`
Byrd R., Lu P., Nocedal J., Zhu C., 1995, SIAM Journal on Scientific Computing, 16, 1190
Davis D. R., Hayes W. B., 2014, ApJ, 790, 87
Díaz-García S., Salo H., Knapen J. H., Herrera-Endoqui M., 2019, arXiv e-prints, p. arXiv:1908.04246
Dobbs C., Baba J., 2014, Publ. Astron. Soc. Aust., 31
Gadotti D. A., 2011, MNRAS, 415, 3308
Gao H., Ho L. C., 2017, ApJ, 845, 114
Gao H., Ho L. C., Barth A. J., Li Z.-Y., 2018, ApJ, 862, 100
Hart R. E., et al., 2016
Hart R. E., et al., 2017, MNRAS, 472, 2263
Head J. T. C. G., Lucey J. R., Hudson M. J., 2015, MNRAS, 453, 3729
Holincheck A. J., et al., 2016
Hopkins P. F., et al., 2010, The Astrophysical Journal, 724, 915
Jacob J. C., et al., 2010, arXiv e-prints, p. arXiv:1005.4454
Jones E., Oliphant T., Peterson P., et al., 2001, SciPy: Open source scientific tools for Python, `http://www.scipy.org/`
Kormendy J., Drory N., Bender R., Cornell M. E., 2010, The Astrophysical Journal, 723, 54
Kruk S. J., et al., 2017, MNRAS, 469, 3363
Kruk S. J., et al., 2018, MNRAS, 473, 4731
Lackner C. N., Gunn J. E., 2012, MNRAS, 421, 2277
Lange R., et al., 2016, MNRAS, 462, 1470
Lintott C. J., et al., 2008, Monthly Notices of the Royal Astronomical Society, 389, 1179
Lupton R., Blanton M. R., Fekete G., Hogg D. W., O'Mullane W., Szalay A., Wherry N., 2004, PUBL ASTRON SOC PAC, 116, 133
Masters K. L., the Galaxy Zoo Team 2019, arXiv e-prints, p. arXiv:1910.08177
Masters K. L., et al., 2010, Monthly Notices of the Royal Astronomical Society, 411, 2026
Mendez-Abreu J., et al., 2016
Park C., Choi Y.-Y., Vogeley M. S., III J. R. G., Blanton M. R., the SDSS collaboration F., 2007, ApJ, 658, 898
Pedregosa F., et al., 2011, Journal of Machine Learning Research, 12, 2825
Peng C. Y., Ho L. C., Impey C. D., Rix H.-W., 2002, AJ, 124, 266
Peng C. Y., Ho L. C., Impey C. D., Rix H.-W., 2010, AJ, 139, 2097
Pour-Imani H., Kennefick D., Kennefick J., Davis B. L., Shields D. W., Abdeen M. S., 2016, The Astrophysical Journal, 827, L2
Pozzetti L., et al., 2009, Astronomy & Astrophysics, 523, A13
Robotham A. S. G., Taranu D. S., Tobar R., Moffett A., Driver S. P., 2016
Salo H., et al., 2015, ApJS, 219, 4
Sanchez S. F., et al., 2011, Astronomy and Astrophysics, 538, A8
Simard L., et al., 2002a, ASTROPHYS J SUPPL S, 142, 1
Simard L., et al., 2002b, The Astrophysical Journal Supplement Series, 142, 1
Simard L., Mendel J. T., Patton D. R., Ellison S. L., McConnachie A. W., 2011, ApJS, 196, 11
Simmons B. D., et al., 2017, MNRAS, 464, 4420
Simpson R., Page K. R., De Roure D., 2014, in Proceedings of the 23rd International Conference on World Wide Web. WWW '14 Companion. ACM, New York, NY, USA, pp 1049–1054, doi:10.1145/2567948.2579215, `http://doi.acm.org/10.1145/2567948.2579215`
Stoughton C., et al., 2002, AJ, 123, 485
The Astropy Collaboration et al., 2018, AJ, 156, 123
Vika M., Bamford S. P., Häußler B., Rojas A. L., 2014, Monthly Notices of the Royal Astronomical Society, 444, 3603
Willett K. W., et al., 2013

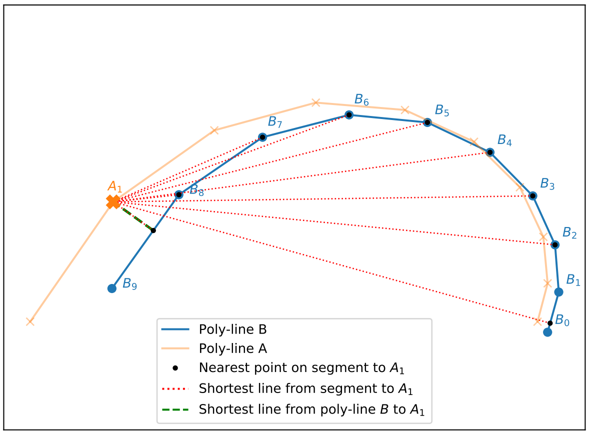

Figure A1. Illustration of the metric used. For each point in line A, the shortest distance to each segment in line B is calculated (shown as dotted red lines). The minimum of these distances (corresponding to the line shown in dashed green) is squared.

Willett K. W., et al., 2017, MNRAS, 464, 4176
Zaninetti L., 2014, arXiv e-prints, p. arXiv:1401.0287
de Vaucouleurs G., de Vaucouleurs A., Corwin Jr. H. G., Buta R. J., Paturel G., Fouqué P., 1991, Third Reference Catalogue of Bright Galaxies. Volume I: Explanations and references. Volume II: Data for galaxies between 0^h and 12^h. Volume III: Data for galaxies between 12^h and 24^h.

APPENDIX A: MATHEMATICAL DESCRIPTION OF THE POLY-LINE SEPARATION MEASURE

This appendix details the metric used in Section 2.6.2 to cluster polylines used by volunteers to model spirals arms. It can be seen as a variant of the Fréchet distance. The metric is illustrated in Figure A1.

First, define a poly-line containing n 2D cartesian coordinates (vertices) as

$$A : \{i \in \mathbb{N};\ i < n\} \longrightarrow \mathbb{R}^2 \tag{A1}$$

We also define a function, t, which calculates how far a point $\vec{p}$ is along the line between two other points ($\vec{v}$ and $\vec{w}$):

$$t(\vec{p},\, \vec{v},\, \vec{w}) \equiv \frac{(\vec{p} - \vec{v}) \cdot (\vec{v} - \vec{w})}{|\vec{w} - \vec{v}|^2}. \tag{A2}$$

The minimum distance from $\vec{p}$ to the line segment between $\vec{v}$ and $\vec{w}$ is given by

$$d(\vec{p},\, \vec{v},\, \vec{w}) = \|\ (\vec{v} + \min(\max(t(\vec{p},\, \vec{v},\, \vec{w}),\, 0),\, 1)\ (\vec{w} - \vec{v})) - \vec{p}\| \tag{A3}$$

We then define a "squared distance" from the poly-line A (containing n vertices) to the poly-line B (containing m vertices):

$$D(A,\, B) \equiv \frac{1}{n}\sum_{i=0}^{n} \min\{j \in \mathbb{N}_0,\ j < m;\ d(A_i,\, B_j,\, B_{j+1})^2\}. \tag{A4}$$

The choice to square the distances and penalize large deviations from other lines was a data-driven choice to improve the results of clustering.

Finally, we define our separation measure between two drawn poly-lines as

$$distance(A,\, B) \equiv D(A,\, B) + D(B,\, A). \tag{A5}$$

APPENDIX B: STACKING OF MULTIPLE SDSS FRAMES

All data required for sigma image creation for stacked frames came from the corrected frames, as detailed in the frame datamodel[10]. For each pixel in an SDSS frame, we have

$$\frac{I}{C} = \frac{n}{g} - S + V, \tag{B1}$$

where I represents the sky-subtracted, corrected image (nanomaggies), C reprents the calibration image, n is the number of electrons captured, g is the gain, S is the Sky value (data units) and V is the dark current, $V = 0\sqrt{v}$ (v being the dark variance).

Given Poisson error,

$$\sigma_n = \sqrt{n}. \tag{B2}$$

If we stack multiple frames, given N observations of a pixel

$$\begin{aligned} n_{\text{total}} &= \sum_i n_i = \sum_i g_i \left(\frac{I_i}{C_i} + S_i - V_i\right), \\ &= \sum_i \frac{g_i}{C_i} I_i + \sum_i g_i\,(S_i - V_i) = \sigma^2_{n_{\text{total}}}. \end{aligned} \tag{B3}$$

This is ideal, and is the level that many fitting software packages work at, we, however, want to return to working in units of nanomaggies on a stacked image, and so further calculation is needed:

$$I = \frac{1}{N}\sum_i I_i, \tag{B4}$$

$$I = \frac{1}{N}\sum_i C_i \left(\frac{n_i}{g_i} - S_i + V_i\right), \tag{B5}$$

And so

$$\sigma_I^2 = \frac{1}{N^2}\sum_i \frac{C_i^2}{g_i^2}\sigma^2_{n_i} + \frac{1}{N^2}\sum_i C_i^2 \sigma^2_{S_i} + \frac{1}{N^2}\sum_i C_i^2 \sigma^2_{V_i}. \tag{B6}$$

We treat the sky value as a constant, such that $\sigma^2_{S_i} = 0$. Substituting $\sigma^2_{n_i} = n_i$ as above gives

$$\sigma_I^2 = \frac{1}{N^2}\sum_i \frac{C_i^2}{g_i^2} n_i + \frac{1}{N^2}\sum_i C_i^2 v_i. \tag{B7}$$

[10] `https://data.sdss.org/datamodel/files/BOSS_PHOTOOBJ/frames/RERUN/RUN/CAMCOL/frame.html#example`

$$\sigma_I = \frac{1}{N}\sqrt{\sum_i C_i^2\left(\frac{n_i}{g_i^2} + v_i\right)}. \tag{B8}$$

Note that this is identical to saying

$$\sigma_I^2 = \frac{1}{N^2}\sum_i \sigma_{I_i}^2. \tag{B9}$$

APPENDIX C: ANCILLARY TABLES

This paper has been typeset from a TEX/LATEX file prepared by the author.

Table C1. The maximum, minimum and default values for model parameters. Note that some parameters were allowed to overflow when fitting, for instance an axis ratio greater 1 (signifying a swap of major and minor axis) was allowed, and corrected for once fitting reached completion. This helped avoid the optimizer encountering parameter bounds and failing to converge. Component roll was similarly unconstrained.

Component	Parameter	Tuning Minimum Bound	Tuning Maximum Bound
disc	μ_x	-inf	inf
	μ_y	-inf	inf
	roll	-inf	inf
	q	0.01	100
	R_e	0	inf
	Σ_e	0	inf
bulge	μ_x	-inf	inf
	μ_y	-inf	inf
	roll	-inf	inf
	q	0.01	100
	R_e	0	inf
	Σ_e	0	inf
	n	0.1	10
bar	μ_x	-inf	inf
	μ_y	-inf	inf
	roll	-inf	inf
	q	0.01	100
	R_e	0	inf
	Σ_e	0	inf
	n	0.1	10
	c	0.01	10
spiral	Σ_e	0	inf
	spread	0	inf
	falloff	0.01	inf

Table C2. Pivot table of reported errors on parameters for our sample of 297 galaxies. Errors quoted are absolute errors.

component	parameter	count	mean	std	min	25%	50%	75%	max
disk	Σ_e (nmgy)	291	0.20	0.21	0.01	0.07	0.14	0.25	1.22
	r_e	291	0.65	0.32	0.08	0.42	0.60	0.85	1.82
	μ_x (arcseconds)	291	0.43	0.28	0.05	0.24	0.38	0.56	2.56
	μ_y (arcseconds)	291	0.44	0.26	0.11	0.26	0.36	0.54	1.93
	b/a	291	0.09	0.04	0.01	0.06	0.09	0.12	0.20
	ϕ (radians)	291	1.63	0.36	0.21	1.43	1.58	1.77	2.93
bulge	Σ_e (nmgy)	272	0.75	0.96	0.00	0.16	0.39	0.85	6.75
	r_e	272	0.08	0.05	0.00	0.05	0.07	0.10	0.47
	μ_x (arcseconds)	272	0.13	0.08	0.00	0.09	0.12	0.16	0.72
	μ_y (arcseconds)	272	0.13	0.07	0.00	0.09	0.11	0.16	0.51
	n	272	1.23	0.64	0.00	0.63	1.40	1.73	2.48
	b/a	272	0.10	0.05	0.00	0.07	0.10	0.14	0.23
	ϕ (radians)	272	1.56	0.57	0.00	1.28	1.57	1.86	3.47
bar	Σ_e (nmgy)	92	0.31	0.39	0.00	0.06	0.16	0.39	2.36
	r_e	92	0.16	0.12	0.02	0.06	0.14	0.20	0.87
	c	92	0.28	0.20	0.00	0.14	0.25	0.42	0.82
	μ_x (arcseconds)	92	0.23	0.26	0.04	0.11	0.17	0.27	2.24
	μ_y (arcseconds)	92	0.24	0.20	0.02	0.13	0.18	0.31	1.09
	n	92	0.37	0.30	0.00	0.08	0.30	0.66	0.88
	b/a	92	0.09	0.04	0.01	0.06	0.08	0.11	0.23
	ϕ (radians)	92	0.69	0.98	0.00	0.06	0.10	1.17	3.57